Dynamics of the two-frequency torus breakdown in the driven double scroll circuit

M. S. Baptista* and I. L. Caldas
Institute of Physics, University of São Paulo, Caixa Postal 66318, CEP 05315-970 São Paulo, São Paulo, Brazil
(Received 3 February 1997; revised manuscript received 6 April 1998)

In this work we numerically identify three scenarios for the two-frequency torus breakdown to chaos, using the driven double scroll circuit, with varying driving parameters. Two of these scenarios follow the Curry-Yorke route to chaos. For one scenario, we identify the transition to chaos through the onset of a heteroclinic tangle and its heteroclinic points. In the other scenario, chaos appears via period-doubling bifurcations. The third scenario is through the type-II intermittency for which a quasiperiodic torus grows in size, breaks by touching external saddle points, and forms a heteroclinic saddle connection. These dynamic scenarios have distinct structure evolutions: for the Curry-Yorke route, chaos appears softly and alternates with phase locking, while, for the type-II intermittency, chaos appears abruptly and is preserved for a large range of the varying driving parameter. [S1063-651X(98)05210-6]

PACS number(s): 05.45.+b

I. INTRODUCTION

The routes to chaos, found in nonlinear systems by varying control parameters, are important because they are used to predict the transition from regular to irregular oscillations [1,2]. One well known example of route to chaos is the infinite sequence of period-doubling bifurcations [3,4], universal for a large class of one varying parameter systems.

Another possible route is the destabilization of the three-frequency torus [5]. This route has a dynamical scenario, through which chaos can appear just after the third Hopf bifurcation, i.e., after the appearance of a third frequency into the system [6,7]. In this case, an arbitrarily small perturbation can lead to the destabilization of a three-frequency oscillation. However, for other scenarios, a three-frequency quasiperiodic movement can also persist under a large perturbation [8–10]. Indeed, chaos is more likely to appear when there is a higher number of frequencies [9].

Moreover, chaos can also occur directly through a destabilization of a two-frequency torus as proposed by Curry and Yorke [11,12]. This general route happens through different scenarios leading to typical folds and wrinkles in the broken torus. In this particular situation chaos can appear for two-parameter families of maps of the plane, through the destabilization of a two-frequency phase-locked trajectory [13,14]. After chaos appears, topological alterations are responsible for the loss of the smoothness of the two-frequency torus. In the same route, chaos also emerges from two-frequency torus through the period-doubling scenario [15]. In this case, a phase-locked band chaos comes into sight with a rational rotation number.

Most of the literature about the two-frequency torus breakdown does not address the topological transitions induced by the driving parameters. These transitions are difficult to recognize in dissipative systems since the homoclinic and heteroclinic tangles contract along the stable direction. References [13,14] contain an overview of the possible topological transitions for the two-frequency torus breakdown to chaos.

In this paper we report dynamical scenarios for the route to chaos found numerically for a driven electronic circuit. Our investigation is motivated by the relevance of the observed two-frequency torus breakdown to the general dynamical systems theory.

We deal with Matsumoto's electronic circuit [16] (also known as Chua's circuit) perturbed sinusoidally. This is a simple nonlinear circuit with a piecewise-linear resistor that has been studied because of its electronic simplicity and variety of nonlinear phenomena. The driven versions of this circuit have been extensively investigated, and many bifurcation phenomena (not observed in the nonperturbed circuit) have been found [17–23].

The onset of chaos by torus breakdown in Matsumoto's circuit, describing a chaotic attractor known as double scroll [24]), and driven by a sinusoidally perturbation, was investigated in Refs. [17,20]. In this case, this circuit is known as the driven double scroll circuit. However, no topological or dynamical analysis is presented, and until now the scenarios for the appearance of chaos by torus breakdown in the driven double scroll circuit remains unknown.

We show that chaos appears by the Curry-Yorke route through period-doubling or phase-locking scenarios. We also show that chaos preceded by phase locking is due to the transversal cross of the strong stable foliations with the stable manifolds of the nodes in the phase-locked trajectory.

In addition, we find that chaos, in the considered driven circuit, can also appear through type-II intermittency [21]. In this paper, a dynamical scenario for this destabilization is proposed, where the two-frequency quasiperiodic torus loses its stability by touching external saddle points that form a heteroclinic saddle connection. This nonlinear mechanism [25] is responsible for the reinjection necessary for the existence of type-II intermittency. Thus, in the driven double scroll circuit, chaos appears in two observable ways, characterized by distinct Lyapunov exponent evolutions and topological changes as a driving parameter is varied. For the Curry-Yorke route, these transitions occur softly in contrast with the hard transitions associated to type-II intermittency.

*Present address: Institute for Plasma Research, University of Maryland, College Park, MD 20742.

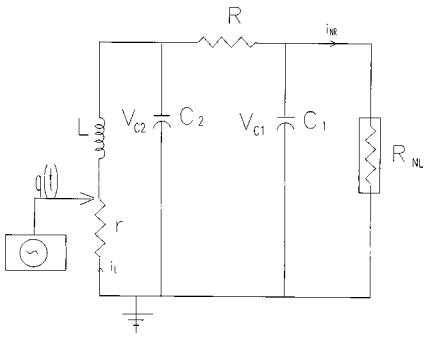

FIG. 1. The double scroll circuit. The electronic value components used in this paper are $C_1=0.0052$ μF, $C_2=0.056$ μF, $R=1470$ Ω, $L=9.2$ mH, and $r=10$ Ω.

Details about the driven double scroll circuit are present in Sec. II. In Sec. III we dynamically analyze the Curry-Yorke route to the onset of chaos in this circuit. In Sec. IV we present the scenario for which chaos appears, in the same circuit, through a type-II intermittency, and conclusions are given in Sec. V.

II. DRIVEN DOUBLE SCROLL CIRCUIT

The double scroll circuit [16] is shown in Fig. 1 with its three energetic components: two capacitors, C_1 and C_2, and one inductor, L. It also has two resistors R and r, and the nonlinear resistor $R_{\rm NL}$, whose characteristic curve is shown in Fig. 2.

The $R_{\rm NL}$ characteristic curve is mathematically represented by

$$i_{NR}(V_{c1})=m_0V_{c1}+0.5(m_1-m_0)|V_{c1}+B_p| +0.5(m_0-m_1)|V_{c1}-B_p|. \quad (1)$$

The driving force applied across the resistor r is represented by

$$q(t)=V\sin(2\pi ft), \quad (2)$$

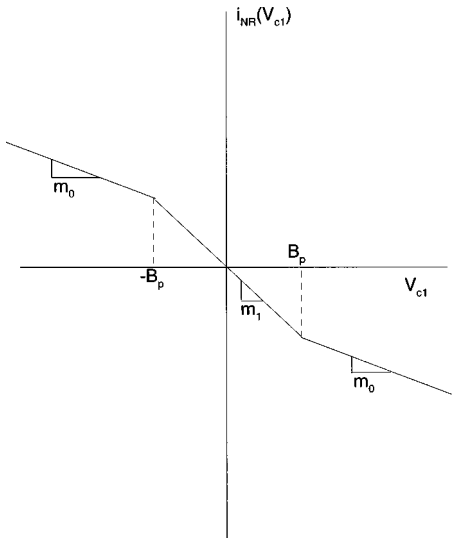

FIG. 2. The characteristic curve of the nonlinear resistor $R_{\rm NL}$, where $B_p=1.0$, $m_0=-0.5$, and $m_1=-0.8$.

where V is the amplitude and f is the frequency.

We can simulate the circuit of Fig. 1 by applying Kirchoff's laws with the resulting state equations

$$C_1\frac{dV_{C1}}{dt}=\frac{1}{R}(V_{C2}-V_{C1})-i_{NR}(V_{c1}),$$

$$C_2\frac{dV_{C2}}{dt}=\frac{1}{R}(V_{C1}-V_{C2})+i_L, \quad (3)$$

$$L\frac{di_L}{dt}=-V_{C2}-q(t),$$

where V_{C1} and V_{C2} are the voltage across the capacitors C_1 and C_2, respectively, and i_L is the electric current across the inductor L.

To avoid numerical problems we rescale Eqs. (3) generating dimensionless variables (V_{C1},V_{C2},i_L) and parameters (C_1,C_2,L,R). The dimensionless values of these parameters, calculated in terms of the real values (given in Fig. 1), are $1/C_1=10.0$, $1/C_2=1.0$, $1/L=6.0$, and $1/R=0.6$. The initial conditions are $V_{c1}(0)=0.152\,64$, $V_{c2}=-0.022\,81$, and $i_L(0)=0.381\,27$, and the step size was $dt=0.005$. For integrating Eqs. (3) we used the fourth-order Runge-Kutta algorithm.

For these parameter simulation values, and null perturbing amplitude $V=0$, the circuit behaves chaotically. As the circuit is dissipative, its dynamic variables (V_{C1}, V_{C2}, and i_L) evolve on a chaotic attractor called double scroll [16].

One of the most known tools for measuring chaos is the Lyapunov spectrum formed, in this case, by three Lyapunov exponents λ_n. Thus, for the considered system, depending on the values of $(\lambda_1,\lambda_2,\lambda_3)$, we can characterize the nature of the attractor as follows: $(+,0,-)$, a chaotic attractor; $(0,0,-)$, a quasiperiodic movement on a torus T^2; $(0,-,-)$, a limit cycle; and $(-,-,-)$, a fixed point. We computed the three Lyapunov exponents, but we present only the first one, because our main interest is to determine how chaotic the system is. The Lyapunov exponents were computed by applying the Eckmann-Ruelle algorithm [12,26], with a transient $n=100$, and a time step $dt=0.005$ during an integration time $t=3882$ which corresponds to $n\approx 700$. The Gram-Schmidt orthonormalization was applied every ten steps. Due to the imprecise computation of these exponents, we consider the first Lyapunov exponent positive if $\lambda_1\gtrsim 0.005$, within the numerical precision considered.

All results presented in this paper are the product of numerical simulations. Complementary information about the considered experiments are given in Ref. [21].

III. SOFT APPEARANCE OF CHAOTIC MOTION

A dynamical overview of the Curry-Yorke route can be seen (for a rising frequency f and a fixed amplitude V) in the bifurcation diagram of Fig. 3(A), and by analyzing the first Lyapunov exponent of Fig. 3(B). These figures show phase locking of quasiperiodic tori, onset of chaos, and further phase-locking alternating with chaotic motion. For the considered parameters, the Lyapunov exponent increases slowly with f. For f close to 0.1978, the exponent reaches a value $\lambda\gtrsim 0.05$, after which phase locking is no longer observed.

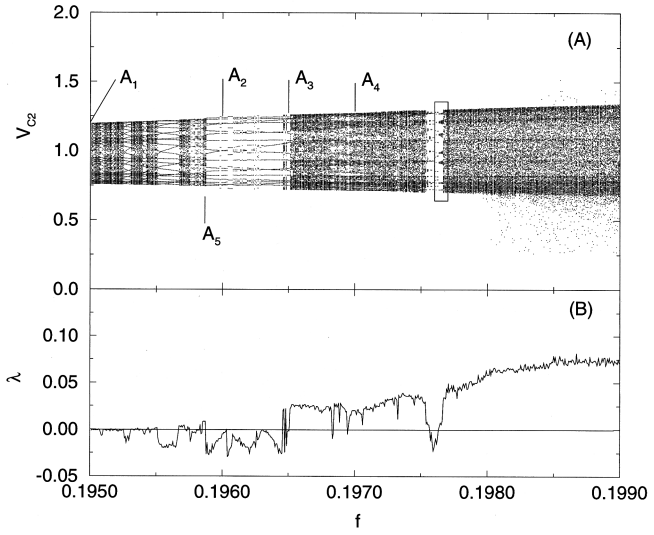

FIG. 3. (A) A bifurcation diagram for a rising amplitude f and a fixed driving amplitude $V=0.20$, showing that phase-locked regions come into sight within quasiperiodic regimes and also in the chaotic regimes. We indicated five regions on which we will focus our analysis. In A_1 we have a quasiperiodic attractor, in A_2 a period-17 phase-locked attractor which coexists with other period-N attractors, in A_3 and A_4 we have the onset of chaos through phase-locking, and in A_5 we have one of the regions where we find weak chaos. (B) The first Lyapunov exponent λ, for the same parameters of (A). That means chaos for $\lambda>0$. $V_{C1}=-1.5$.

The four regions indicated in Fig. 3(A), denoted by A_1, A_2, A_3, and A_4, have their corresponding attractors shown on the Poincaré sections of Fig. 4. Thus, Fig. 4(A) shows the quasiperiodic attractor indicated by A_1 in Fig. 3(A). Figure 4(B) shows the period-17 phase-locked attractor indicated by A_2 in Fig. 3(A). Finally, Figs. 4(C) and 4(D) show the chaotic attractor indicated by A_3 and A_4 in Fig. 3(A).

As we see in Fig. 3(B), after the onset of chaos, the first Lyapunov exponent increases slowly with f. Additionally, the chaotic trajectory obtained in the Curry-Yorke scenario is

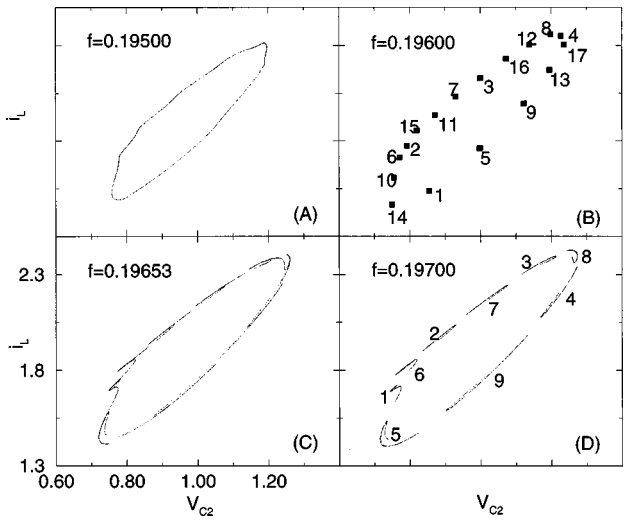

FIG. 4. (A) Quasiperiodic two-frequency torus (region A_1 in Fig. 3), (B) Period-17 phase-locking (region A_2 in Fig. 3), a chaotic attractor with many folds (region A_3 in Fig. 3), and a nine-band chaotic attractor (region A_4 in Fig. 3). $V_{C1}=-1.5$.

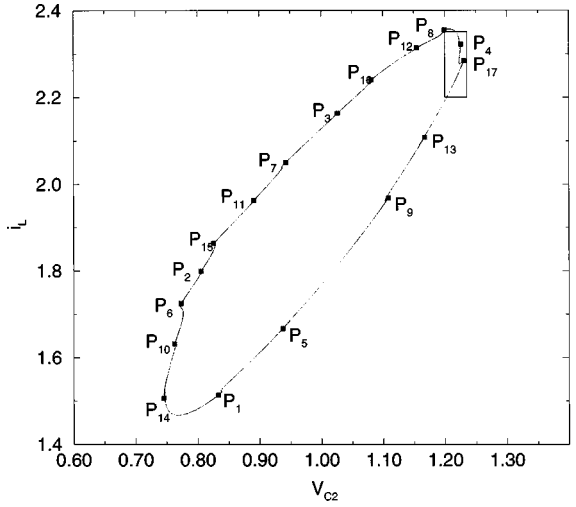

FIG. 5. Poincaré section of the chaotic attractor for f indicated by A_5 in Fig. 3.

confined to the region previously occupied by the previous stable quasiperiodic torus. Only for higher values of f does the trajectory escape the toroidal surface neighborhood. Because of these characteristics, we refer to this transition as a soft onset of chaos.

In Fig. 4(C) we see that the smooth and closed quasiperiodic attractor [in Fig. 4(A)], after phase-locking [Fig. 4(B)] and the onset of chaos, becomes a folded and rough attractor. Further amplifications of these folds reveal a fractal structure, and also the stretching and folding characteristics of chaotic regimes. In this case, chaos can be better recognized by analyzing the geometric structure of the attractor than by computing the Lyapunov exponent. Consequently, this procedure could be considered when the first Lyapunov coefficient values cannot be distinguished from zero.

However, in the case of Fig. 4(D), a small amplification already reveals the mentioned geometric properties. This figure shows also a phase-unlocked, nine-band, chaotic attractor. The evolution of the region n is given by the region $n+1$. Thus, we clearly see that region 2 is the region 1 folded along a direction transversal to the torus, and stretched along a direction tangent to the torus surface.

The observed folding and stretching processes and the computed Lyapunov exponent assure us that the trajectory is chaotic. However, we want to see how the transition from a phase-locked trajectory to the chaotic trajectory happens. For this purpose we analyze the attractor when (for the used numerical precision) we first observe the onset of chaos. In Fig. 5 we see a toroidal-shaped attractor, which actually is chaotic. Although the Lyapunov exponent is positive, its value is very small. Thus, in this example, chaos should not be characterized by analyzing only this exponent, and a geometric interpretation of this toroidal-shaped attractor must also be considered for characterizing the transition to chaos.

Before the onset of chaos shown in Fig. 5 happens, the period-17 phase-locked attractor is the only attractor observed. To examine the influence of this attractor on the transition to chaos, in Fig. 6 we examine the amplification of the box in Fig. 5, particularly the geometry nearby the unstable period-17 attractor.

To guide that, let us introduce a mapping G that models

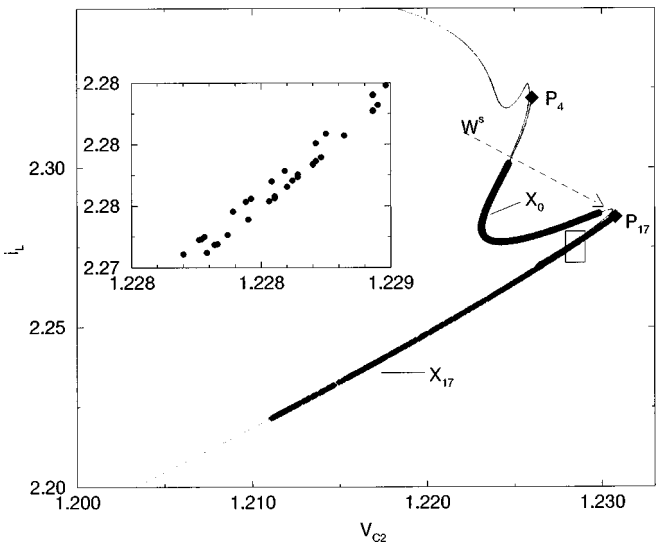

FIG. 6. Magnification of Fig. 5 showing a region (large gray line) X_0 that after 17 Poincaré section crossings is transformed into the region X_{17}. So X_0 stretches along the unstable manifold of the point P_{17}, and folds along the stable manifold of this point. Within the box we see a magnification of the region X_{17}.

the trajectory in the Poincaré section of Fig. 5. If we consider each period-17 unstable point represented by P_n (with $n=1,\ldots,17$), then, $G^{17}(P_n)=P_n$, and $G(P_n)=P_{n+1}$. In addition, for the case shown in Fig. 5, G is a counterclockwise-oriented chaotic rotation. This means that given a point P in between, for example, P_4 and P_{17}, forward iterations of P by G^{17} leads to P_{17}. The reason for the existence of this chaotic-oriented rotation will be explained later in this paper, and is a consequence of the geometric patterns behind the onset of chaos.

To identify the chaotic characteristics of the trajectory shown in Fig. 5, in Fig. 6 we plot the region around the points P_4 and P_{17}. The points in the large black region denoted by X_0, when iterated by $G^{17}(X_0)$, rest in the large black region denoted by X_{17}. The small box in this last region is magnified and we see that the region X_{17} is in fact composed of two regions. The region X_0 under the mapping G suffers a stretching along the unstable manifold W^u, and a fold along the stable direction W^s (corresponding to the strong stable foliation, represented in Fig. 7), transversal to W^u at the point P_{17}. The onset of chaos is due to the appearance of a horseshoe in the vicinity of each of the 17 points that compose the period-17 orbit, the skeleton that sustains chaos.

Indeed, the chaotic torus that we see in Fig. 5 lies in W^u, and the period-17 orbit is one of the infinite unstable periodic orbits that a chaotic system possesses. However, this is a very special orbit because there is a heteroclinic orbit connecting this periodic orbit, and thus there is chaos around this period-17 orbit.

For a varying driving parameter, we see that chaos actually appears from a period-17 phase-locked trajectory that is seen in the Poincaré section as 17 nodes. Between each two of these nodes, there is one saddle point. The unstable manifolds of these saddle points direct the trajectory toward these nodes. The manner in which the unstable manifolds of these saddle points cross the stable manifolds of the nodes causes

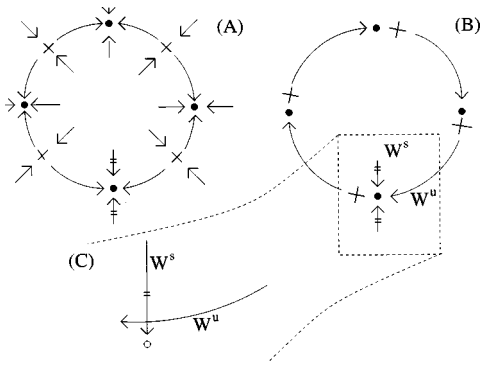

FIG. 7. (A) The phase-locked torus with four saddle points (crosses) and four nodes (filled circles). (B) The saddle points approaching the nodes in an uncounterclockwise direction. Inside the dashed box we see the stable manifold of the node, the strong stable foliation W^s (marked with double lines), and the unstable manifold of a saddle point W^u. (C) Transversal crossing of W^u with W^s, creating a horseshoe.

the appearance of a horseshoe around the 17 points of the period-17 trajectory.

To illustrate the geometrical scenario for the onset of chaos from a periodic orbit (soft transition), suppose that instead of a period-17 orbit we have a period-4 phase-locked trajectory, as shown in Fig. 7(A). In this figure, we represent the phase-locked period-4 trajectory (the nodes) by circles, and the saddle points by crosses. The strong stable foliations are the stable manifolds both of the saddles and of the nodes in the transversal direction. A strong stable foliation of one node (the lower one in this figure) is indicated by small double lines in Fig. 7.

The existence of the saddle points are due to a saddle-node bifurcation that creates the phase-locked trajectory, from a quasiperiodic torus. Just before the phase-locked trajectory loses its stability (that happens in the driven double scroll circuit due to changes in the driving parameters, *f* or *V)* we observe that the saddle points approach the nodes as shown in Fig. 7. Eventually, the saddle points and the nodes collide (an inverse saddle-node bifurcation) and then a quasiperiodic torus is created.

However, another situation may arise, the onset of chaos. In this case, the unstable manifold of one saddle point [indicated in Fig. 7(B) by W^u] transversally crosses the strong stable foliation [indicated in Fig. 7(B) by W^s] of one node as shown in Fig. 7(C) [a magnification of the box in Fig. 7(B)], creating a horseshoe around this point. The existence of this scenario has been theoretically predicted in Ref. [13].

Note that the saddle points in Fig. 7(B) go toward the nodes in a noncounterclockwise rotation. As a consequence, their unstable manifolds that appear with chaos and cross the strong stable foliation are counterclockwise oriented. This causes a counterclockwise-oriented chaotic trajectory to appear. In Fig. 5, we show a case where the trajectory evolves in time following a counterclockwise-oriented rotation. However, we also have observed chaotic noncounterclockwise oriented rotation, in the driven double scroll circuit. In this case, the approach of the saddle points toward the nodes occurs in a counterclockwise direction. This oriented rotation disappears for a parameter far from the critical value for which the transition to chaos occurs.

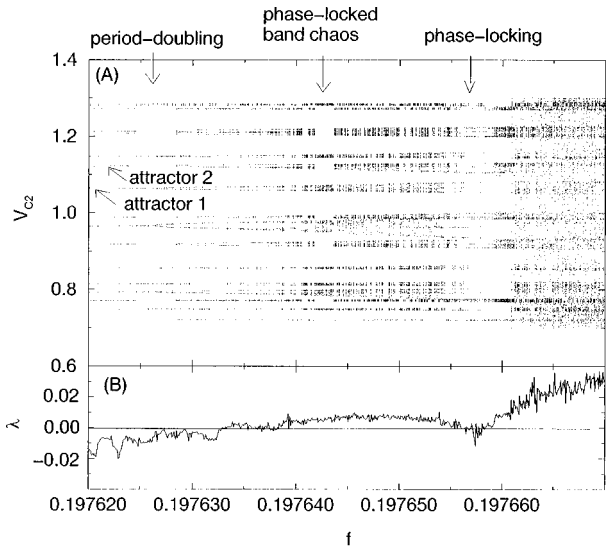

FIG. 8. (A) Bifurcation diagram showing coexistence of attractors and the onset of chaos through period doubling, by a rising driving frequency f and a fixed driving amplitude $V=0.20$. (B) The first Lyapunov exponent λ, for the same parameters of (A). $V_{C1}=-1.5$.

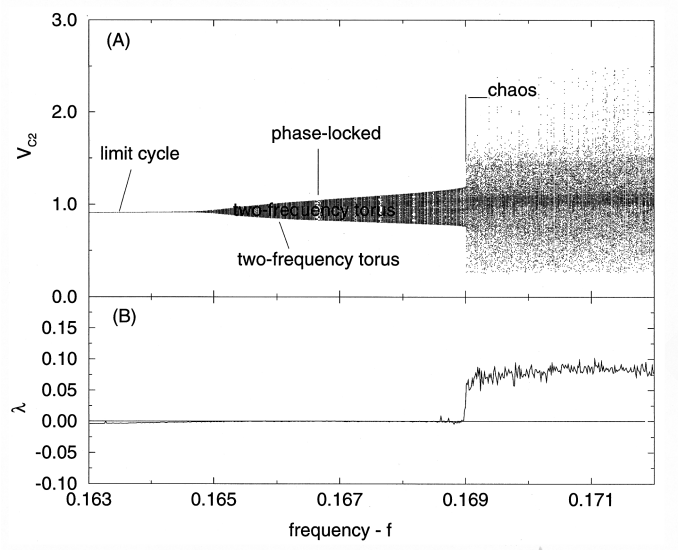

FIG. 10. (A) Bifurcation diagram showing the two-frequency torus creation (via Hopf bifurcation) and its destruction, generating chaotic behavior, by a rising driving frequency f and a fixed driving amplitude $V=0.28$. (B) The first Lyapunov exponent λ, for the same parameters of (A). $V_{C1}=-1.5$.

After the onset of chaos, phase-locked trajectories might still appear due to the occurrence of a saddle-node bifurcation. Furthermore, chaos can also appear through an infinite sequence of period-doubling bifurcations, as seen in Fig. 8. After that, chaotic bands appear with very small Lyapunov coefficients. The Lyapunov exponent increases its value when the bands merge in only one chaotic band. In Fig. 8 we also see the coexistence of two attractors [23] indicated by attractors 1 and 2.

The spectral analysis of the soft onset of chaos is shown in Fig. 9. Figure 9(A) shows the spectrum for the double scroll circuit ($V=0$). We see two main peaks, one corresponding to the characteristic frequency $f_c \cong 0.29$ [23] and the other, indicated by f_1, corresponding to the frequency with which the trajectory jumps between the two rolls presented in the double scroll attractor [16]. For $f=0.185\,00$ and $V=0.20$, in Fig. 9(B), the peaks at f_1 and f_c are destroyed and a peak f corresponding to the driving frequency appears (the manner in which they are destroyed can be seen in Ref. [23]). Increasing the frequency to $f=0.195\,00$ another incommensurable frequency f_2 appears and thus we have a quasiperiodic movement. In Fig. 9(D) the frequencies f and f_2 become commensurable, and so phase locking occurs. A low amplitude broadband appears in Fig. 9(E), revealing a chaotic attractor, also observed in Figs. 9(F) and 9(G). Note that Figs. 8(C)–8(F) correspond respectively to Figs. 4(A)–4(D).

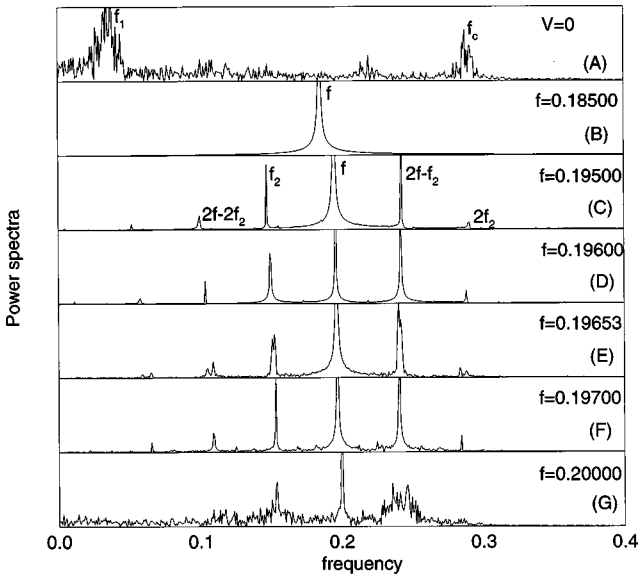

FIG. 9. Power spectra of the time evolution of the variable V_{C1}. Spectra of the nonperturbed circuit (A) and for varying driving frequency and fixed driving amplitude $V=0.20$; phase locking in (B), quasiperiodic oscillation in (C), phase locking (D), and chaos in (E), (F), and (G).

IV. ABRUPT APPEARANCE OF CHAOTIC MOTION

The abrupt appearance of chaos, via two-frequency torus breakdown, has been investigated through numerical integration of Eqs. (3), for a fixed driving amplitude $V=0.28$. Thus Fig. 10(A) shows a bifurcation diagram of the variable V_{C2}, when the trajectory crosses a Poincaré section at $V_{C1}=-1.5$, as a function of the driving frequency, f. The abrupt appearance of chaos, seen in this figure, is confirmed by the first Lyapunov exponent λ [Fig. 10(B)]. Chaos first appears for $f=0.168\,97$, leading to $\lambda>0$.

In this bifurcation diagram, there are no periodic orbits after the onset of chaos. In addition, the first Lyapunov exponent has a large value at the onset of chaos, which is preserved by increasing the frequency f.

For increasing values of f and V fixed, in Fig. 11 we see a sequence of four figures showing the modifications in the attractor on the Poincaré section at $V_{C1}=-1.5$. The two-frequency torus (T^2) is created after a supercritical Hopf

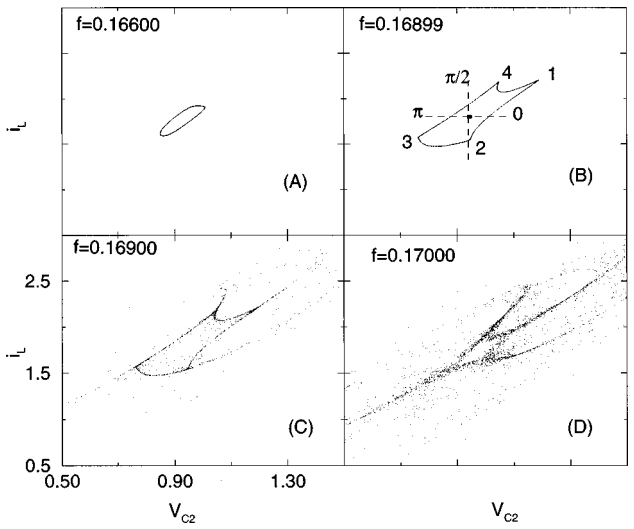

FIG. 11. (A) A quasiperiodic torus T^2 for $f=0.166\,00$. (B) The four-sided quasiperiodic folded torus for the critical parameter $f=0.168\,99$. (C) The destruction of the torus, leading to a type-II intermittency. (D) A chaotic attractor with a heteroclinic saddle disconnection for $f=0.170\,00$. $V=0.28$ and $V_{C1}=-1.5$.

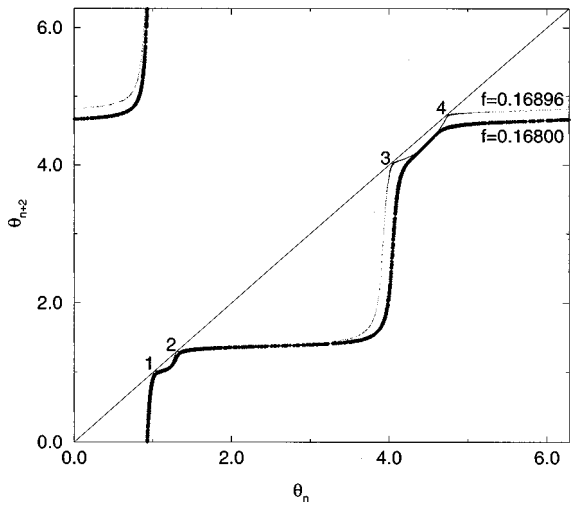

FIG. 12. Angular period-2 return map for two values of the parameter f indicated in figure. This is evidence that, increasing f, the torus grows in size, approaching two period-2 saddle points.

bifurcation. In this situation, before the onset of chaos, the torus is a deformed circle with no folds or cuspides, as shown in Fig. 11(A) ($f=0.166\,00$). However, increasing the frequency to $f=0.168\,99$, the torus T^2 grows in size and folds in four parts resembling a four-sided polygon [Fig. 11(B)]. The torus breaks as shown in Fig. 11(C) ($f=0.169\,00$) leading to the appearance of type-II intermittency [21]. This causes the trajectory to evolve spirally around the previously existing repelor focus point, localized close to the origin of the angular frame in Fig. 11(B). Further increasing the frequency, we can hardly recognize the previous existing torus [Fig. 11(D)].

In Fig. 11(B) the four folds of the T^2 torus can be recognized by the numbers 1, 2, 3, and 4. These folds are approaching four invisible saddle points (whose positions could be determined by introducing noise); each pair of saddle points represents a period-2 basic cycle. So, in the vicinity of the fold 4, there is an invisible basic cycle that crosses the section again near the fold 2. The same occurs to the other folds, and the cycle crosses from fold 3 to fold 1. Along the torus, not yet destroyed, a quasiperiodic trajectory is counterclockwise oriented with a winding number ($w=0.4806\ldots$) close to the rational fraction $w=\frac{12}{25}$. Twelve is the number of the trajectory rotations along the torus to go back near the same point, taking 25 complete poloidal cycles.

In Fig. 11(C), after passing near each saddle point, the trajectory crosses this Poincaré section two times before returning to the same saddle point. We can consider the flow on this section as a mapping G. So, if c_n where $n=1,\ldots,4$ are the saddle points, then $G^2(c_n)=c_n$, $G(c_4)=c_2$, and $G(c_3)=c_1$.

As a matter of fact, the laminar spiral trajectory is a four-spiral trajectory, which means that the trajectory visits one of the four spirals each time . These spirals evolve approaching the saddle points asymptotically [Fig. 11(C)]. In fact, each spiral tends to one of the four corners of the polygon. These corners, indicated by numbers, reach the saddle points when chaos appears. These saddle points have two different unstable manifolds. Along one unstable manifold of the saddle point the trajectory is ejected outside the polygon, causing a chaotic burst, characteristic of intermittent regimes [21]. Along the other unstable manifold the trajectory is directed to the nearest saddle point in the counterclockwise direction, i.e., $G^2(c_4+\epsilon)$ leaves c_4 to c_1, for example.

The angular frame shown in Fig. 11(B) is used to locate the four folds in an angular space. So, in Fig. 12, the angular period-2 return map shows that before the torus breaks ($f=0.168\,00$) there is no angular two period-2 fixed points as shown by the large black line (although the large line seems to touch the identity straight line, it does not). However, just before the torus breaks ($f=0.168\,96$), we see that two period-2 fixed points are formed by an infinitesimal increase of the parameter f.

Figure 13 shows a sketch of the flow of the mapping G^2. We see in Fig. 13(A) the stable two-frequency torus and the

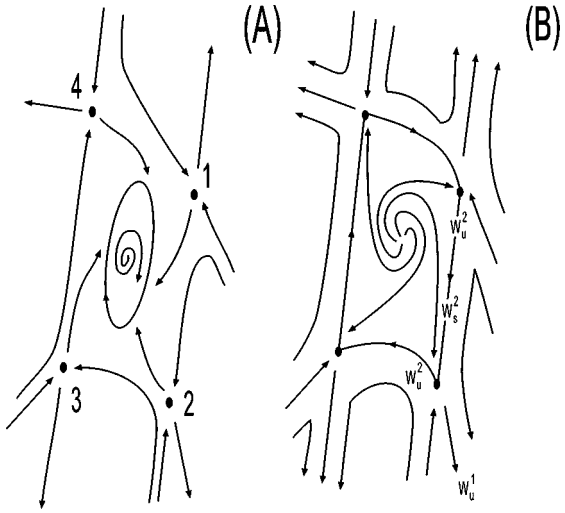

FIG. 13. The geometry behind the torus breakdown. In this figure we see the flow of the mapping G^2 for the stable two-frequency torus (A) and for its breakdown forming the heteroclinic saddle connection (B).

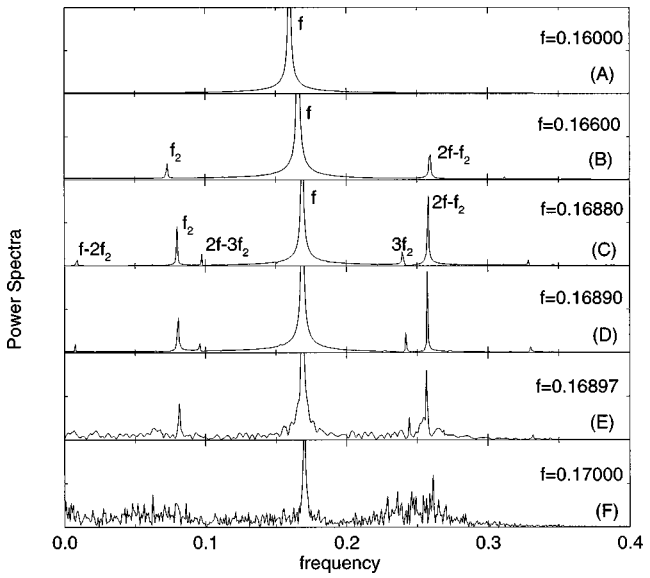

FIG. 14. Sequence of power spectra, indicating phase locking (A), quasiperiodic two-frequency tori [(B), (C), and (D)], onset of chaos (E), and a large chaotic band (F).

surrounding invisible four saddle points. Then the torus grows in size, folding and touching the four saddle points. After the torus touches these points [Fig. 13(B)], it is no longer closed (since its breakdown has already occurred); the saddle points become visible and form a heteroclinic saddle connection [25]. This heteroclinic saddle connection is the nonlinear mechanism responsible for the chaotic burst and reinjection around the repelor focus, typical of type-II intermittent behavior [21].

After the heteroclinic saddle connection is created, further increasing the frequency generates the heteroclinic saddle disconnection where there is no longer the spiraling laminar behavior of the trajectory around the repelor focus. In fact, each of the four spirals turns into four straight lines. This means that, after the trajectory is reinjected around the repelor focus, it approaches the saddle points along an oriented straight line, and there is no more spiraling.

The unstable manifolds responsible for the chaotic burst are indicated in Fig. 13(B) by W_u^1, and those responsible for the heteroclinic saddle connection (an orbit in G^2 that connects the two period-2 saddle points) are indicated by W_u^2. So the unstable manifold of the saddle point 1 [indicated in Fig. 13(A)], $W_u^2(1)$, is the stable manifold of point 3 [indicated in Fig. 12(B)], $W_s^2(3)$. This heteroclinic loop is also called a Poincaré homoclinic contour [27].

Amplifications of regions in the vicinity of points 1–4 show that, in fact, we have a horseshoe surrounding these points due to transversal crossings between W^u and W^s. However, for the sake of simplicity we have not shown these crossings in Fig. 13.

In Fig. 14 we see a sequence of power spectra for a limit cycle [Fig. 14(A)] with frequency f, that suffers a Hopf bifurcation with the appearance of a second frequency f_2, originating a quasiperiodic two-frequency tori [Figs. 14(B)–14(D)] only with frequencies $nf+mf_2$ $(n,m \in \mathbb{N})$. Furthermore, in Fig. 14(E) we see the onset of chaos, and in Fig. 14(F) a large chaotic band. So we see in these spectra that for a very small change in the driving parameter, a large chaotic band appears. This is different from the soft onset of chaos for which a large parameter variation is required in order to make these chaotic bands noticeable.

V. CONCLUSIONS

We have numerically analyzed the oscillations and the onset of chaos induced in the sinusoidally driven double scroll circuit. For varying driving parameters, the attractors are identified by power spectrum analyses, and by computing bifurcation diagrams and the first Lyapunov exponent. We also describe topological changes due to the onset of chaos through two-frequency torus breakdown.

We show that in the driven double scroll circuit chaos can appear directly through the breakdown of a two-frequency torus when a parameter is varied. Furthermore, we identified three possible scenarios for this transition: two in the Curry-Yorke route, and one through type-II intermittency.

First, we find that, for the system considered in this work, the torus can softly break to chaos through the route of Curry and Yorke [11]. One scenario for this route is when phase-locked trajectories become unstable and heteroclinic chaos appears, as generally proposed in Ref. [13]. Moreover, in this case we identify the geometry (a transversal crossing of the strong stable foliation with the unstable manifold of a saddle point) in the vicinity of the heteroclinic point (the phase-locked trajectory that loses its stability). This is difficult to realize for a dissipative system like the driven double scroll circuit. Second, another identified scenario for the onset of chaos in the Curry-Yorke route is the period-doubling bifurcations, like for instance for the driven p-n junction passive resonators circuit [15].

We have recently identified another scenario for the onset of chaos in the analyzed circuit [21], namely, the abrupt appearance of chaos through type-II intermittency. In this scenario, a two-frequency quasiperiodic torus loses its stability by touching the saddle points and forming a heteroclinic saddle connection. We identify this as the nonlinear mechanism responsible for the reinjection of the trajectory, around the repelor focus that produces the laminar phase of the type-II intermittency.

These identified two-frequency torus breakdowns to chaos, for a varying parameter, have two distinct dynamic characteristics. Chaos appears softly in the Curry-Yorke route, through phase-locking and period-doubling scenarios, and after the onset of chaos, phase-locking is again observed due to a saddle-node bifurcation. On the other hand, via type-II intermittency, chaos appears abruptly and is preserved for a large range of the varying parameter. Furthermore, the two-frequency torus breakdown preceded by a torus doubling, as reported in Refs. [28,29] for other systems, has not been observed in this work.

Generally, the Curry-Yorke route has another possible scenario for the onset of chaos through quasiperiodic two-frequency torus breakdown [14], not yet observed in the driven double scroll circuit. However, this scenario is difficult to observe since the attractors usually phase lock before breaking. This happens because one must appropriately choose two parameter variations to maintain the attractor with the same irrational rotation (Thus avoiding phase lock-

ing). We also have studied the case of fixed driving frequency and varying driving amplitude, in which case the same as above conclusions can be drawn. Finally, the scenarios reported in this paper might be useful to determine other scenarios for torus breakdown observed in other systems with two or more basic frequencies [30].

ACKNOWLEDGMENTS

The authors thank Dr. W. P. de Sá for the computational assistance, and Dr. W. M. Gonçalves, E. F. Manfra, Dr. E. Rosa, and K. Hebble for revising the manuscript. This work was partially supported by FAPESP and CNPq.

[1] E. Ott, *Chaos in Dynamical Systems* (Cambridge University Press, Cambridge, 1993).
[2] K. T. Alligood, T. D. Sauer, and J. A. Yorke, *Chaos, an Introduction to Dynamical Systems* (Springer, New York, 1997).
[3] M. L. Feigenbaum, J. Stat. Phys. **19**, 25 (1978).
[4] A. Libchaber, C. Laroche, and S. Fauve, J. Phys. (France) Lett. **43**, L211 (1982).
[5] D. Ruelle and F. Takens, Commun. Math. Phys. **20**, 167 (1971).
[6] J. P. Gollup and H. L. Swinney, Phys. Rev. Lett. **35**, 927 (1975).
[7] H. L. Swinney and J. P. Gollub, Phys. Today **31** (8), 41 (1978).
[8] P. S. Linsay and A. W. Cumming, Physica D **40**, 196 (1989).
[9] C. Grebogi, E. Ott, and J. A. Yorke, Physica D **15**, 354 (1984).
[10] P. M. Battelino, Phys. Rev. A **38**, 1495 (1988).
[11] J. H. Curry and J. A. Yorke, Lect. Notes Math. **688**, 48 (1978).
[12] P. Bergé, *Le Chaos: Théorie et Experiences* (Eyrolles, Paris, 1988).
[13] D. G. Aronson, M. A. Chory, G. R. Hall, and R. P. McGehee, Commun. Math. Phys. **83**, 303 (1982).
[14] S. Ostlund, D. Rand, J. Sethna, and E. Siggia, Physica D **8**, 303 (1983).
[15] R. V. Buskirk and C. Jeffries, Phys. Rev. A **31**, 3332 (1985).
[16] T. Matsumoto and L. O. Chua, IEEE Trans. Circuits Syst. **CAS-32**, 797 (1985).
[17] M. Itoh, H. Murakami, and L. O. Chua, Int. J. Bifurcation Chaos Appl. Sci. Eng. **4**, 1721 (1994).
[18] K. Murali and M. Lakshmanan, Int. J. Bifurcation Chaos Appl. Sci. Eng. **2**, 621 (1992).
[19] L. Pivka, A. L. Zheleznyak, and L. O. Chua, Int. J. Bifurcation Chaos Appl. Sci. Eng. **4**, 1743 (1994).
[20] K. Murali and M. Lakshmanan, Int. J. Bifurcation Chaos Appl. Sci. Eng. **1**, 369 (1991).
[21] M. S. Baptista and I. L. Caldas (unpublished).
[22] M. S. Baptista, Ph.D. thesis, University of São Paulo, São Paulo, IFUSP, 1996.
[23] M. S. Baptista and I. L. Caldas, Nonlinear Dynamics (to be published).
[24] S. Hayes, C. Grebogi, and E. Ott, Phys. Rev. Lett. **70**, 3031 (1993).
[25] D. K. Arrowsmith and C. M. Place, *An Introduction to Dynamical Systems* (Cambridge University Press, London, 1990).
[26] J. P. Eckmann and D. Ruelle, Rev. Mod. Phys. **57**, 617 (1985).
[27] L. P. Shil'nikov, Int. J. Bifurcation Chaos Appl. Sci. Eng. **4**, 489 (1994).
[28] H. Tominaga and H. Mori, Prog. Theor. Phys. **91**, 1081 (1994).
[29] J. Simonet, E. Brun, and R. Badii, Phys. Rev. E **52**, 2294 (1995).
[30] V. S. Anishchenko, M. A. Safonova, U. Feudel, and J. Kurths, Int. J. Bifurcation Chaos Appl. Sci. Eng. **4**, 595 (1994).